Generic Multi-output Spectral Representation Method for Uncertainty Propagation Analysis of Power System Dynamics

Zhaoyuan Wang, *Graduate Student Member*, *IEEE*, and Siqi Bu, *Senior Member*, *IEEE*

***Abstract*—Realistic uncertainties of renewable energies and loads may possess complicated probability distributions and correlations, which are difficult to be characterized by standard probability density functions and hence challenge existing uncertainty propagation analysis (UPA) methods. Also, nonintrusive spectral representation (SR)-based UPA methods can only estimate system responses at each time point separately, which is time-consuming for analyzing power system dynamics. Thus, this paper proposes a generic multi-output SR (GMSR) method to effectively tackle the above limitations by developing the generic correlation transformation and multi-output structure. The effectiveness and superiority of GMSR in efficiency and accuracy are demonstrated by comparing it with existing SR methods.**

***Index Terms*—Probabilistic stability, renewable energy, spectral representation, power system dynamics, uncertainty.**

I. Introduction

RECENTLY, increasing uncertainties in power systems induced by high penetration of renewable energies pose a huge threat to system stability [1]. Thus, effective uncertainty propagation analysis (UPA) methods for power system dynamics aiming at calculating the probability distributions of system dynamic responses caused by uncertainties are in pressing need.

UPA methods can be mainly categorized into three types, including numerical methods, analytical methods, and approximation methods. Among numerical methods, Monte Carlo simulation (MCS) is one of the most widely applied methods in power system dynamics. Although there are some techniques to improve the sampling efficiency of MCS, e.g., Latin hypercube sampling, Halton sampling, and Sobol sampling [2], thousands of simulations are normally required, which is time-consuming. By comparison, analytical methods significantly improve efficiency. Among analytical methods, Taylor series expansion needs derivative operations, and convolution methods require independent uncertainty inputs, which only have limited applications in power systems [3], [4]. By comparison, point estimation methods and cumulant-based methods are applied in power systems more widely [1]. However, as pointed out in [5], they cannot guarantee the accuracy in calculating the probability distributions of system dynamic responses. Thus, numerical methods and analytical methods have drawbacks in efficiency and accuracy, respectively.

The emerging approximation methods provide solutions that balance efficiency and accuracy. Gaussian process regression is based on Bayesian inference [2]. However, the kernel functions of Gaussian process regression need to be preselected based on experience, and the computational complexity is high. By comparison, spectral representation (SR) has been applied in power system dynamics more widely, mainly including low-rank approximation (LRA) and polynomial chaos expansion (PCE) [1], [5]. However, there are still some obstacles to the further broad application of SR. The first one is that most SR methods can only estimate the system dynamic response at each time point separately, restricted by the single output [5]-[8], whereas UPA for power system dynamics focuses on the system dynamic response at all time points during the concerned period of time. This means that massive SR models need to be constructed, which is cumbersome and time-consuming. Although some SR methods with multiple outputs have been proposed based on Galerkin [9], [10], they are intrusive, which means that they need the complicated transformation for power system state-space equations and all the detailed structure and parameters of power systems, which are difficult to measure in reality accurately. The second limitation is that SR methods require independent uncertainties as inputs, and correlated uncertainties should be transformed into independent ones firstly. Most uncertainty transformation methods are based on Rosenblatt or Nataf transformations [5]-[7], which require that the joint probability distributions of uncertainties can be accurately characterized, or the joint probability distributions

Manuscript received: June 9, 2024; revised: October 2, 2024; accepted: December 2, 2024. Date of CrossCheck: December 2, 2024. Date of online publication: January 30, 2025.

This work was supported in part by the National Natural Science Foundation of China (No. 52077188), and in part by the Hong Kong Research Grant Council (No. 15208323).

Z. Wang is with the Department of Electrical and Electronic Engineering, The Hong Kong Polytechnic University, Hong Kong, China (e-mail: zhaoyuan.wang@connect.polyu.hk).

S. Bu (corresponding author) is with the Department of Electrical and Electronic Engineering, Shenzhen Research Institute, Research Centre for Grid Modernisation, International Centre of Urban Energy Nexus, Centre for Advances in Reliability and Safety, Research Institute for Smart Energy, and Policy Research Centre for Innovation and Technology, The Hong Kong Polytechnic University, Hong Kong, China (e-mail: siqi.bu@polyu.edu.hk).

DOI: 10.35833/MPCE.2024.000586

can be approximated by existing Copula functions. However, for complicated uncertainties in reality, these assumptions may not be guaranteed. Although there are some data-driven uncertainty transformation methods, e. g., principal component analysis-based methods [11], [12], they can only ensure the transformed uncertainties are uncorrelated rather than independent.

Therefore, to overcome the above limitations, this paper proposes a UPA method named generic multi-output spectral representation (GMSR) for power system dynamics. The major contributions can be summarized as follows.

1) The proposed GMSR has multiple outputs and thus can estimate system dynamics at different time points simultaneously, which significantly improves efficiency. Also, as a nonintrusive method, GMSR only needs the measurements of uncertainties and system dynamic responses.

2) It is discovered by case studies that the realistic uncertainties of renewable energies and loads may not be accurately modeled by standard probability distributions and have complicated correlations. The uncertainty transformation included in GMSR can effectively transform uncertainties with arbitrary correlations into independent ones only based on measurements of uncertainties and without any priori knowledge, which is the fundamental step for SR methods.

3) The proposed GMSR integrates the merits of existing SR methods, including being applicable to uncertainties with arbitrary probability distributions and having sparse structure, thereby avoiding the curse of dimensionality.

4) As a universal UPA method, the proposed GMSR can be applied to various probabilistic stability issues of power systems related to system dynamics and thus has wide applications.

II. Methodology Description

Uncertainties of renewable energies and loads are widely concerned in power systems and thus are considered in this paper. The proposed GMSR utilizes weight summation of spectral functions to approximate the relationship $\boldsymbol{M}(\boldsymbol{\xi})$ between independent uncertainties $\boldsymbol{\xi}$ and the system response $\boldsymbol{y}=[y(\Delta t),\ldots,y(i\Delta t),\ldots,y(T_{\mathrm{d}})]^{\mathrm{T}}$ with T_{d} as the concerned time period of system dynamic response and Δt as the step length.

$$\boldsymbol{y}=\boldsymbol{M}(\boldsymbol{\xi})\approx\hat{\boldsymbol{y}}=\hat{\boldsymbol{M}}(\boldsymbol{\xi})=\boldsymbol{W}\boldsymbol{\varphi}(\boldsymbol{\xi})=\left[\sum_{j=1}^{N_{\mathrm{r}}}\boldsymbol{\omega}_{1j}\varphi_j(\boldsymbol{\xi}),\ldots,\sum_{j=1}^{N_{\mathrm{r}}}\boldsymbol{\omega}_{ij}\varphi_j(\boldsymbol{\xi}),\ldots,\sum_{j=1}^{N_{\mathrm{r}}}\boldsymbol{\omega}_{N_y j}\varphi_j(\boldsymbol{\xi})\right]^{\mathrm{T}} \tag{1}$$

where N_{r} is the number of representation items; the subscript $N_y=T_{\mathrm{d}}/\Delta t$ denotes the number of GMSR outputs $\boldsymbol{y}$; the superscript ˆ represents the approximation derived from GMSR; $\varphi_j(\boldsymbol{\xi})$ is the j^{th} item of spectral function $\boldsymbol{\varphi}(\boldsymbol{\xi})$, which denotes the spectral function arranged in ascending order; and $\boldsymbol{\omega}_{ij}$ is the entry in i^{th} row and j^{th} column of the weight coefficient matrix $\boldsymbol{W}$.

From (1), one of the major differences between the form of GMSR and that of the existing nonintrusive SR is that GMSR has multiple outputs, whereas the existing nonintrusive SR only has one output. Also, according to (1), the main tasks of deriving GMSR model can be summarized as: ① transformation of correlated uncertainties into independent ones $\boldsymbol{\xi}$; ② construction of spectral function $\boldsymbol{\varphi}(\boldsymbol{\xi})$; and ③ calculation of weight coefficient matrix $\boldsymbol{W}$. It should be noted that $\boldsymbol{W}$ is directly derived in GMSR as a whole rather than calculating $\boldsymbol{\omega}_i$ separately and combining them into $\boldsymbol{W}$. Otherwise, (1) is only a combination of the existing nonintrusive SR models. Additionally, GMSR relies on the sampling data of uncertainties and system dynamic responses, which can be obtainable in realistic power systems [13], [14]. Moreover, many existing studies on UPA are based on the premise that the data of uncertainties and system dynamic responses are obtainable [6]-[9]. Thus, data reliance will not limit the application of GMSR.

A. Generic Transformation for Correlated Uncertainties

There are similarities between uncertainty transformation and blind source separation. In detail, correlated uncertainties are similar to the observed and mixed signals in blind source separation. And transforming correlated uncertainties into independent ones is similar to restoring the observed signals to the original ones. Thus, the methods with blind source separation have the potential to be used in uncertainty transformation. And the basic idea of independent component analysis (ICA) that can effectively separate mixed signals into uncorrelated and independent signals is applied in this paper.

For a set of correlated uncertainties after centering $\boldsymbol{\varsigma}=[\varsigma_1,\varsigma_2,\ldots,\varsigma_{N_{\mathrm{c}}}]^{\mathrm{T}}$, where N_{c} is the number of correlated uncertainties, N_{s} sampling data of $\boldsymbol{\varsigma}$ are expressed as $\boldsymbol{\varsigma}^{(1\sim N_{\mathrm{s}})}$. Firstly, whitening processing is conducted to transform the correlated uncertainties into uncorrelated ones $\tilde{\boldsymbol{\varsigma}}$ with unit variance based on eigenvalue decomposition, which can be formulated as:

$$\tilde{\boldsymbol{\varsigma}}^{(1\sim N_{\mathrm{s}})}=\boldsymbol{U}\boldsymbol{S}^{-\frac{1}{2}}\boldsymbol{U}^{\mathrm{T}}\boldsymbol{\varsigma}^{(1\sim N_{\mathrm{s}})} \tag{2}$$

where $\boldsymbol{U}$ is the right eigenvector of $\boldsymbol{\varsigma}^{(1\sim N_{\mathrm{s}})}(\boldsymbol{\varsigma}^{(1\sim N_{\mathrm{s}})})^{\mathrm{T}}$. The diagonal entries of $\boldsymbol{S}$ are the eigenvalues of $\boldsymbol{\varsigma}^{(1\sim N_{\mathrm{s}})}(\boldsymbol{\varsigma}^{(1\sim N_{\mathrm{s}})})^{\mathrm{T}}$.

Then, based on ICA, the transformation from uncorrelated uncertainties into independent ones can be regarded as finding a transformation matrix $\boldsymbol{B}=[\boldsymbol{b}_1,\boldsymbol{b}_2,\ldots,\boldsymbol{b}_{N_{\mathrm{c}}}]^{\mathrm{T}}$ that can maximize the non-Gaussianity [15], which can be formulated as:

$$\begin{cases}\max\limits_{\boldsymbol{B}}\sum\limits_{n=1}^{N_{\mathrm{c}}}(\boldsymbol{E}(G(\boldsymbol{b}_n^{\mathrm{T}}\tilde{\boldsymbol{\varsigma}}^{(1\sim N_{\mathrm{s}})}))-\boldsymbol{E}(G(\upsilon)))^2\\ \text{s.t. }\boldsymbol{E}((\boldsymbol{b}_{n'}^{\mathrm{T}}\tilde{\boldsymbol{\varsigma}}^{(1\sim N_{\mathrm{s}})})\circ(\boldsymbol{b}_{n''}^{\mathrm{T}}\tilde{\boldsymbol{\varsigma}}^{(1\sim N_{\mathrm{s}})}))=1\quad n'=n''\\ \qquad\boldsymbol{E}((\boldsymbol{b}_{n'}^{\mathrm{T}}\tilde{\boldsymbol{\varsigma}}^{(1\sim N_{\mathrm{s}})})\circ(\boldsymbol{b}_{n''}^{\mathrm{T}}\tilde{\boldsymbol{\varsigma}}^{(1\sim N_{\mathrm{s}})}))=0\quad n'\neq n''\end{cases} \tag{3}$$

where $\boldsymbol{E}(\cdot)$ is the mean operator; υ is an uncertainty following the standard Gaussian distribution; $G(\cdot)$ is the contrast function, which can be chosen as logcosh; and ∘ is the Hadamard product operator.

To solve (3), the fixed-point algorithm [16], as presented in (4), is used to update $\boldsymbol{b}_n$ iteratively until it converges so that the fast ICA can be implemented.

$$\begin{cases}\boldsymbol{b}_{nv'}=\boldsymbol{E}(\tilde{\boldsymbol{\varsigma}}^{(1\sim N_{\mathrm{s}})}\circ\dot{G}(\boldsymbol{b}_{n(v-1)}^{\mathrm{T}}\tilde{\boldsymbol{\varsigma}}^{(1\sim N_{\mathrm{s}})}))-\boldsymbol{E}(\ddot{G}(\boldsymbol{b}_{n(v-1)}^{\mathrm{T}}\tilde{\boldsymbol{\varsigma}}^{(1\sim N_{\mathrm{s}})}))\boldsymbol{b}_{n(v-1)}\\ \boldsymbol{b}_{nv}=\dfrac{\boldsymbol{b}_{nv'}}{\|\boldsymbol{b}_{nv'}\|_2}\end{cases} \tag{4}$$

where $\dot{G}(\cdot)$ and $\ddot{G}(\cdot)$ are the first- and second-order derivatives of $G(\cdot)$, respectively; $\boldsymbol{b}_{nv}$ and $\boldsymbol{b}_{nv'}$ are the updated $\boldsymbol{b}_n$ at the v^{th} iteration with and without normalization, respectively; and $\|\cdot\|_2$ is the ℓ_2 norm.

After $\boldsymbol{B}$ is calculated, the transformation from correlated uncertainties $\boldsymbol{\varsigma}$ to independent ones $\boldsymbol{\xi}$ can be derived as:

$$\boldsymbol{\xi}=\boldsymbol{B}\boldsymbol{U}\boldsymbol{S}^{-\frac{1}{2}}\boldsymbol{U}^{\mathrm{T}}\boldsymbol{\varsigma} \tag{5}$$

It should be noted that the ICA is only effective when data do not follow Gaussian distributions. And since realistic uncertainties are complicated, they will not strictly follow Gaussian distributions. Thus, this ICA-based uncertainty transformation is universally effective for realistic uncertainties.

B. Construction of Spectral Functions for Uncertainties with Arbitrary Probability Distributions

Spectral functions are formed by orthogonal bases. For the orthogonal basis $\psi^{[j_m]}(\xi_m)$ with respect to ξ_m with the order of j_m, it can be expressed as:

$$\psi^{[j_m]}(\xi_m)=\sum_{n=0}^{j_m}\kappa_n\xi_m^n \quad \kappa_{j_m}=1 \tag{6}$$

where κ_n is the coefficient of ξ_m^n.

To construct bases applicable to uncertainties with arbitrary probability distributions, the orthogonality is used, which is described as:

$$\frac{\sum_{h=1}^{N_s}\psi^{[j_m]}(\xi_m^{(h)})\psi^{[j_q]}(\xi_m^{(h)})}{N_s}=0 \quad 0\le j_q<j_m \tag{7}$$

where j_q indicates the order.

According to (7), when $j_q=0,1$, there is:

$$\begin{cases}\dfrac{\sum_{h=1}^{N_s}\psi^{[j_m]}(\xi_m^{(h)})}{N_s}=0\\ \dfrac{\sum_{h=1}^{N_s}\psi^{[j_m]}(\xi_m^{(h)})(\kappa_0+\xi_m^{(h)})}{N_s}=0\end{cases} \tag{8}$$

Then, the following equation can be derived by substituting the first equation of (8) into the second equation of (8).

$$\frac{\sum_{h=1}^{N_s}\psi^{[j_m]}(\xi_m^{(h)})\xi_m^{(h)}}{N_s}=0 \tag{9}$$

Moreover, the following equation can be derived by substituting $j_q=2,3,\ldots,j_m-1$ in turns into (7) and repeating the above procedure.

$$\frac{\sum_{h=1}^{N_s}\psi^{[j_m]}(\xi_m^{(h)})\xi_m^{j_q,(h)}}{N_s}=0 \quad j_q=0,1,\ldots,j_m-1 \tag{10}$$

According to (10) and (6), when $j_q=j_u-1$, we have:

$$\frac{\sum_{h=1}^{N_s}(\kappa_0+\ldots+\xi_m^{j_m,(h)})\,\xi_m^{j_u-1,(h)}}{N_s}=0 \quad 1\le j_u\le j_m \tag{11}$$

Formula (11) can be rewritten as (12) by defining $\chi_{j_u}=\sum_{h=1}^{N_s}\xi_m^{j_u+j_m-1,(h)}/N_s$, $1\le j_u\le j_m$, $\boldsymbol{\Theta}=[\theta_{j_uj_n}]_{j_m\times j_m}$, $\theta_{j_uj_n}=-\sum_{h=1}^{N_s}\xi_m^{j_u+j_n-2,(h)}/N_s$, $1\le j_u,j_n\le j_m$.

$$\kappa_0\theta_{j_u1}+\kappa_1\theta_{j_u2}+\ldots+\kappa_{j_m-1}\theta_{j_uj_m}=\chi_{j_u} \tag{12}$$

j_m equations similar to (12) can be derived by assigning $j_u=1,2,\ldots,j_m$. Then, these equations are formulated into the matrix form as:

$$[\kappa_0,\kappa_1,\ldots,\kappa_{j_m-1}]^{\mathrm{T}}=\boldsymbol{\Theta}^{-1}[\chi_1,\chi_2,\ldots,\chi_{j_m}]^{\mathrm{T}} \tag{13}$$

After orthogonal bases are determined according to (6) and (13), spectral functions can be constructed. To alleviate the curse of dimensionality, the hyperbolic truncation is introduced. Thus, $\varphi_j(\boldsymbol{\xi})$ can be formed as:

$$\begin{cases}\varphi_j(\boldsymbol{\xi})=\psi^{[j_1]}(\xi_1)\circ\ldots\circ\psi^{[j_m]}(\xi_m)\circ\ldots\circ\psi^{[j_{N_c}]}(\xi_{N_c})\\ \|j_m\|_{c_\gamma}=\left(\sum_{m=1}^{N_c}j_m^{c_\gamma}\right)^{\frac{1}{c_\gamma}}\le N_o\end{cases} \tag{14}$$

where N_o expresses the order of GMSR; and c_γ is the hyperbolic truncation coefficient.

C. Weight Coefficient Calculation

The calculation of $\boldsymbol{W}$ as a whole in (1) can be regarded as the multiple linear regression (MLR), where the sampling data of system dynamic response $\boldsymbol{y}^{(1\sim N_s)}$ and spectral functions $\boldsymbol{\varphi}(\boldsymbol{\xi})^{(1\sim N_s)}$ have already been derived. To avoid overfitting and reduce the complexity of $\boldsymbol{W}$, the form of multi-task elastic net [17] is introduced in calculating $\boldsymbol{W}$, which can be formulated as the following optimization problem:

$$\min_{\boldsymbol{W}}\|\boldsymbol{y}^{(1\sim N_s)}-\boldsymbol{W}\boldsymbol{\varphi}(\boldsymbol{\xi})^{(1\sim N_s)}\|_{\mathrm{F}}^2/2N_s+\lambda\rho\|\boldsymbol{W}\|_{21}+\frac{\lambda}{2}(1-\rho)\|\boldsymbol{W}\|_{\mathrm{F}} \tag{15}$$

where λ is the penalty factor of the complexity of $\boldsymbol{W}$; ρ is the weight coefficient of different norms; and $\|\cdot\|_{\mathrm{F}}$ and $\|\cdot\|_{21}$ are the Frobenius norm and $\ell_1\ell_2$ norm, respectively, which are expressed as:

$$\begin{cases}\|\boldsymbol{A}\|_{\mathrm{F}}=\sqrt{\sum_{kl}a_{kl}^2}\\ \|\boldsymbol{A}\|_{21}=\sum_k\sqrt{\sum_l a_{kl}^2}=\sum_k\|a_k\|_2\end{cases} \tag{16}$$

where a_{kl} is the entry in the k^{th} row and l^{th} column of the indicated matrix $\boldsymbol{A}$.

To solve (15), the coordinate descent algorithm can be used. And the introduction of $\|\boldsymbol{W}\|_{\mathrm{F}}$ in (15) is for avoiding overfitting. The introduction of $\|\boldsymbol{W}\|_{21}$ in (15) is for reducing the ℓ_2 norm of $\boldsymbol{A}$ in every row, which restricts the complexity of $\boldsymbol{W}$ in every row, i.e., ensuring the sparse structure of GMSR, thereby avoiding the curse of dimensionality.

D. Probabilistic Analysis of GMSR Outputs

After deriving the GMSR model in (1), arbitrary moments can be estimated based on the GMSR outputs since its outputs are the values of system dynamic responses under uncertainties with different values. Also, mean μ_i and variance σ_i^2 of $y(i\Delta t)$ are usually concerned in existing studies [7], [8], which are estimated as examples and expressed as:

$$\begin{cases} \hat{\mu}_i = \sum_{h=1}^{N_p} \hat{y}(i\Delta t)^{(h)} / N_p \\ \hat{\sigma}_i^2 = \sum_{h=1}^{N_p} (\hat{y}(i\Delta t)^{(h)})^2 / N_p - \hat{\mu}_i^2 \end{cases} \tag{17}$$

where N_p is the number of sampling data derived from GMSR.

Based on kernel density estimation (KDE), the probability density function (PDF) $p(\cdot)$ of $y(i\Delta t)$ can be estimated as:

$$\hat{p}(\hat{y}(i\Delta t)) = \sum_{h=1}^{N_p} \Phi((\hat{y}(i\Delta t) - \hat{y}(i\Delta t)^{(h)}) / \vartheta_i) / (N_p \vartheta_i) \tag{18}$$

where $\Phi(\cdot)$ is the Gaussian kernel function of KDE; and ϑ_i is the bandwidth of KDE with respect to $y(i\Delta t)$, which can be chosen as $1.06\hat{\sigma}_i N_p^{-0.2}$ [7].

III. Case Study

A. Case 1: IEEE 68-bus 5-area Benchmark System

Case 1 is conducted in IEEE 68-bus 5-area benchmark system [18]. There are 3 wind power generation units (WPG1-WPG3), 3 photovoltaic units (PV1-PV3), and 3 loads with realistic uncertainties based on measurements in [13] connecting at buses 29, 31, 41, buses 6, 10, 36, and buses 27, 47, 48, respectively. The simulation platform is a computer with the hardware of Intel Core i7-8700 CPU @ 3.20 GHz and 16 GB memory and Python as software. The applied simulation models of generators and automatic voltage regulators are simplified 3rd-order model and 1st-order model, separately [19]. To illustrate the probability distributions and the correlations among uncertainties, their PDFs after normalization are drawn, as shown in Fig. 1, and the correlation coefficients of pairwise uncertainties (U1-U9) are listed in the upper triangular units of Table I. The correlation coefficients and the independence hypothesis test results of uncertainties after conducting the uncertainty transformation are listed in the lower triangular units of Table I to show the performance of the uncertainty transformation.

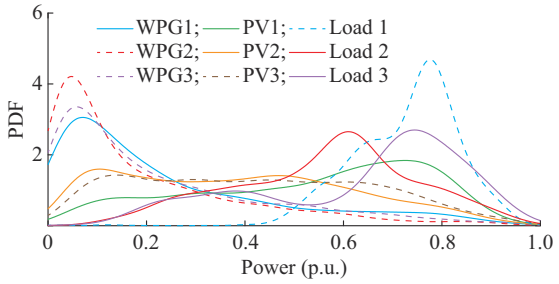

Fig. 1. PDFs of realistic uncertainties.

From Fig. 1, the PDFs of realistic uncertainties are complicated, especially those of PV3 and load 3, the shapes of which are quite different from the standard PDFs. And in Table I, the correlation coefficients between different pairwise uncertainties are various. By comparison, after uncertainty transformation, all correlation coefficients among uncertainties are close to 0, and all independence hypothesis tests are passed. The results demonstrate the effectiveness of the uncertainty transformation in transforming the correlated uncertainty into independent ones.

TABLE I
Correlation Coefficients and Independence Hypothesis Among Uncertainties Before and After Uncertainty Transformation in Case 1

Uncertainty	U1	U2	U3	U4	U5	U6	U7	U8	U9
U1	-	0.01	0.02	–0.24	–0.08	–0.06	0.04	0.16	0.08
U2	0/Y	-	0.54	–0.03	–0.22	–0.25	0.08	0.17	0.09
U3	0/Y	0/Y	-	0.01	–0.30	–0.29	0.15	0.07	0.12
U4	0/Y	0/Y	0/Y	-	0.40	0.41	–0.07	–0.33	–0.14
U5	0/Y	0/Y	0/Y	0/Y	-	0.89	–0.09	–0.47	–0.23
U6	0/Y	0/Y	0/Y	0/Y	0/Y	-	–0.10	–0.48	–0.23
U7	0/Y	0/Y	0/Y	0/Y	0/Y	0/Y	-	0.53	0.82
U8	0/Y	0/Y	0/Y	0/Y	0/Y	0/Y	0/Y	-	0.81
U9	0/Y	0/Y	0/Y	0/Y	0/Y	0/Y	0/Y	0/Y	-

Note: 0/Y denotes that the correlation coefficient is 0, and the independence hypothesis is accepted at a 5% level of significance.

1) Probabilistic Frequency Stability Analysis

GMSR is applied to analyze the system frequency response $f_{sys}(t)$ and area-level frequency response in Area 1 $f_{a1}(t)$ with the trip of the largest infeed generator at 0.1 s, where $T_d = 10$ s, $\Delta t = 0.01$ s. The results of 5000 MCSs are regarded as the baselines [18]. The performance of the proposed GMSR in efficiency and accuracy is compared with those of other SR methods, including sparse PCE (SPCE) and LRA with the setting as: $N_s = 200$, $N_o = 4$ [5], $\lambda = 1/(2N_s)$, $\rho = 0.5$. The selection of λ and ρ is to equally consider the sparsity and generalization. And SPCE is chosen as the comparison method since the conventional PCE is infeasible with the above setting due to the curse of dimensionality.

Firstly, the efficiency of various methods in analyzing $f_{sys}(t)$ is compared, as illustrated in Table II. From Table II, since SPCE, LRA, and GMSR only require 200 simulations, whereas MCS requires 5000 simulations, the simulation time needed for SPCE, LRA, and GMSR is significantly shorter than that needed for MCS. Moreover, the efficiency of GMSR is greatly superior to that of SPCE and LRA. The method execution time of GMSR is more than 40 times shorter than that of SPCE and LRA. The reason is that SPCE and LRA only have one output. To analyze $f_{sys}(t)$ at each time point, $N_y = T_d/\Delta t = 1000$ models are required to be constructed separately. By comparison, GMSR has multiple outputs, and the number of the constructed GMSR model is only 1, indicating the time-saving merit.

TABLE II
Efficiency Comparison of Probabilistic Frequency Stability Analysis in Case 1

Method	Simulation time (s)	Method execution time (s)	Total time (s)
MCS	9852.744	-	9852.744
SPCE	391.659	110.944	502.603
LRA	391.659	101.016	492.675
GMSR	391.659	2.320	393.979

Moreover, the accuracy of various methods in estimating the moments, i. e., mean and standard deviation (Std.), of $f_{\mathrm{sys}}(t)$ and $f_{\mathrm{a1}}(t)$ is compared, as shown in Fig. 2. PDFs of absolute errors (AEs) of moments are introduced to assess overall accuracy, as shown in Fig. 3.

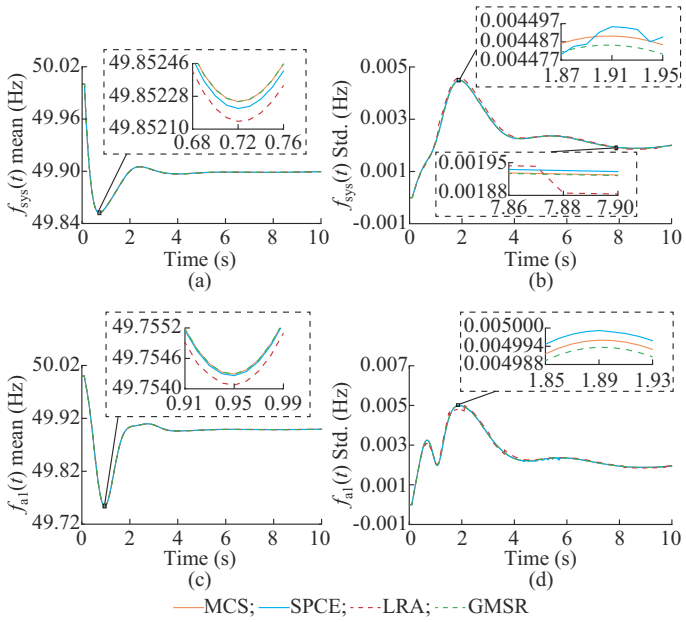

Fig. 2. Accuracy of various methods in estimating moments. (a) $f_{\mathrm{sys}}(t)$ mean. (b) $f_{\mathrm{sys}}(t)$ Std.. (c) $f_{\mathrm{a1}}(t)$ mean. (d) $f_{\mathrm{a1}}(t)$ Std..

According to Fig. 2(a) and (b), for $f_{\mathrm{sys}}(t)$, the overlapping degree between the moment curves derived from MCS and those from GMSR are higher than those from SPCE and LRA. Moreover, from Fig. 2(b), the Std. curve from GMSR is smoother since each time point corresponds to one SPCE or LRA, $\boldsymbol{\omega}_i$ of which is calculated separately.

By comparison, $\boldsymbol{W}$ of GMSR is calculated as a whole. Similar results can be found in Fig. 2(c) and (d) for $f_{\mathrm{a1}}(t)$, where the moment curves derived from GMSR are closer to those from MCS compared with those from SPCE and LRA. Moreover, in Fig. 3, LRA presents the worst performance. And the peaks of PDF of AE associated with $f_{\mathrm{a1}}(t)$ from SPCE are closer to 0 compared with those associated with $f_{\mathrm{sys}}(t)$, which means that the accuracy of SPCE in estimating $f_{\mathrm{a1}}(t)$ is higher than that in estimating $f_{\mathrm{sys}}(t)$. However, its performance is still not as good as that of GMSR. And the PDF of AE from GMSR has higher peaks and thinner tails, the peaks of which are closer to 0. These results indicate that GMSR has higher accuracy in estimating the moments of both system and area-level frequency responses. The reason is that the complicated correlations among realistic uncertainties cannot be transformed accurately in SPCE and LRA, which decreases their estimation accuracy.

Also, to assess the accuracy of various methods in estimating PDFs of frequency responses, AE of PDF, i.e., $|p(f(t))-\hat{p}(\hat{f}(t))|$, is presented in Fig. 4. The shape difference of PDFs ε, i.e., $\varepsilon=\|p(f(t))-\hat{p}(\hat{f}(t))\|_2$, is introduced to assess the overall accuracy, the PDFs of which are drawn in Fig. 5.

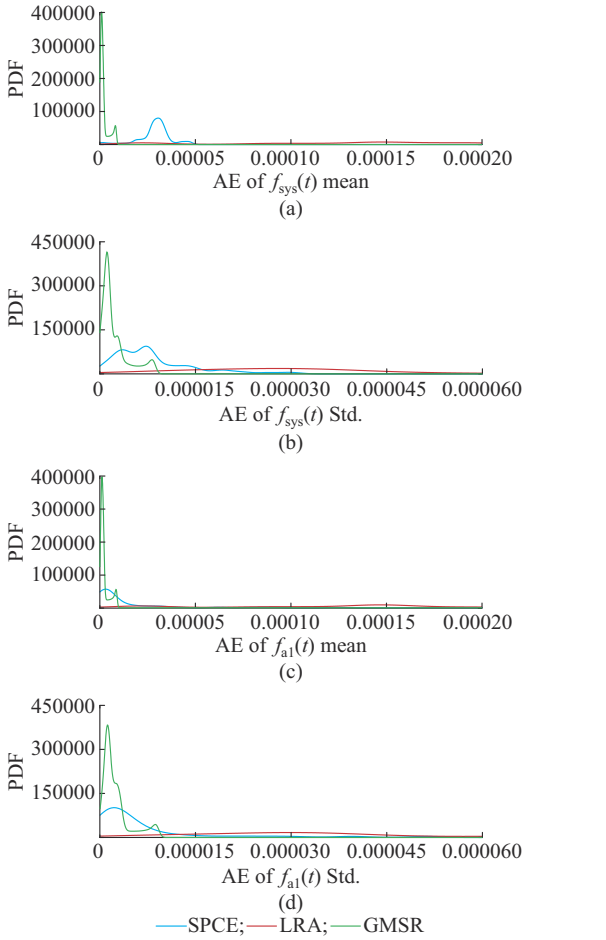

Fig. 3. PDFs of AEs of moments. (a) PDF of AE of $f_{\mathrm{sys}}(t)$ mean. (b) PDF of AE of $f_{\mathrm{sys}}(t)$ Std.. (c) PDF of AE of $f_{\mathrm{a1}}(t)$ mean. (d) PDF of AE of $f_{\mathrm{a1}}(t)$ Std..

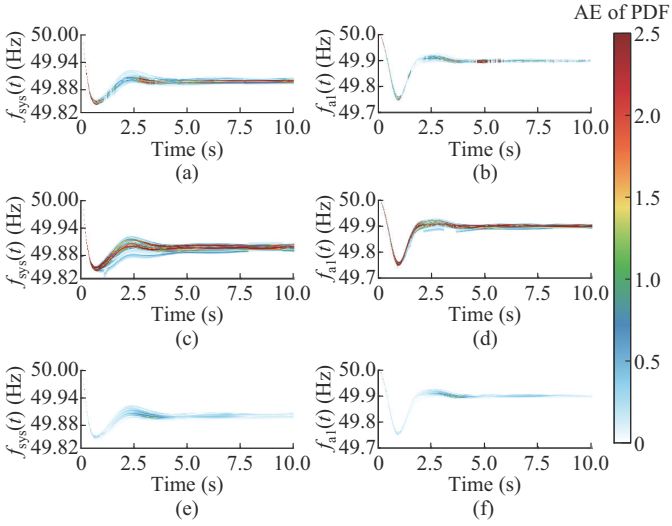

Fig. 4. AEs of PDFs of $f_{\mathrm{sys}}(t)$ and $f_{\mathrm{a1}}(t)$. (a) AE of PDF of $f_{\mathrm{sys}}(t)$ from SPCE. (b) AE of PDF of $f_{\mathrm{a1}}(t)$ from SPCE. (c) AE of PDF of $f_{\mathrm{sys}}(t)$ from LRA. (d) AE of PDF of $f_{\mathrm{a1}}(t)$ from LRA. (e) AE of PDF of $f_{\mathrm{sys}}(t)$ from GMPR. (f) AE of PDF of $f_{\mathrm{a1}}(t)$ from GMSR.

From Fig. 4, the AEs of PDFs of $f_{\mathrm{sys}}(t)$ and $f_{\mathrm{a1}}(t)$ from GMSR are much smaller than those from SPCE and LRA,

which can be observed more clearly from the results at only one time point, as shown in Fig. 5(a) and (c). Moreover, from Fig. 5(b), for $f_{sys}(t)$, the PDF of ε from GMSR has the thinner tail and higher peak closer to 0 at 2.242, whereas the peaks of PDF of ε from SPCE and LRA are at 28.130 and 71.548. Also, from Fig. 5(d), for $f_{a1}(t)$, the peak of PDF of ε from GMSR is at 2.162, and those from SPCE and LRA are at 5.547 and 61.297, respectively. These results indicate the higher accuracy of GMSR in estimating PDFs of both $f_{sys}(t)$ and $f_{a1}(t)$ at different time points.

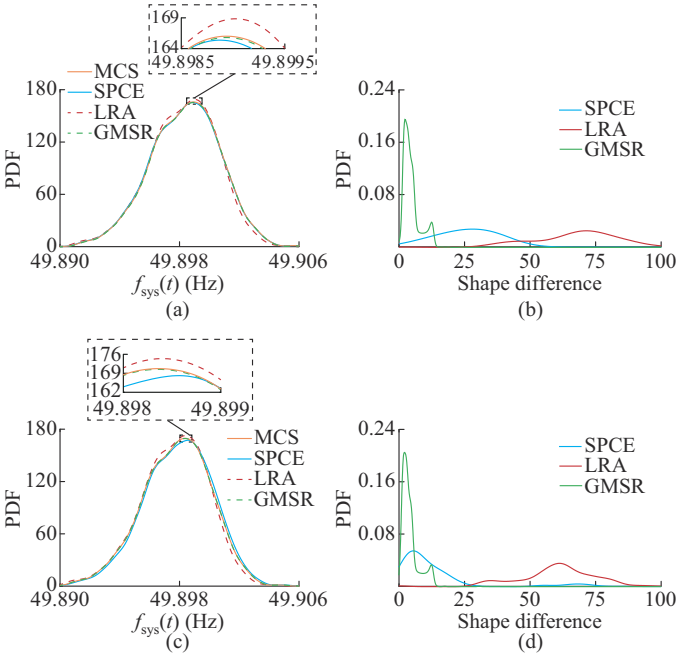

Fig. 5. PDFs of $f_{sys}(t)$ and shape difference. (a) PDF of $f_{sys}(t)$ at $t=5$ s. (b) PDF of ε of $f_{sys}(t)$. (c) PDF of $f_{a1}(t)$ at $t=5$ s. (d) PDF of ε of $f_{a1}(t)$.

2) Probabilistic Transient Stability Analysis

Then, GMSR is applied to analyze the difference between the rotor angle of generator 1 and that of generator 2, denoted as $\delta_{12}(t)$, in the system with a short-circuit fault at bus 16 during 0.1-0.2 s, as an example. It can also be used to analyze the maximal rotor angle difference; however, the results are not shown for saving space. The rest settings are the same as those in the previous section. The efficiency comparison of probabilistic transient stability analysis in Case 1 is presented in Table III. The accuracy comparison of $\delta_{12}(t)$ moment estimation and $\delta_{12}(t)$ PDF estimation among various UPA methods are illustrated in Figs. 6, and 7, respectively.

TABLE III
EFFICIENCY COMPARISON OF PROBABILISTIC TRANSIENT STABILITY ANALYSIS IN CASE 1

Method	Simulation time (s)	Method execution time (s)	Total time (s)
MCS	10243.150	-	10243.150
SPCE	407.539	111.090	518.629
LRA	407.539	101.282	508.821
GMSR	407.539	2.429	409.968

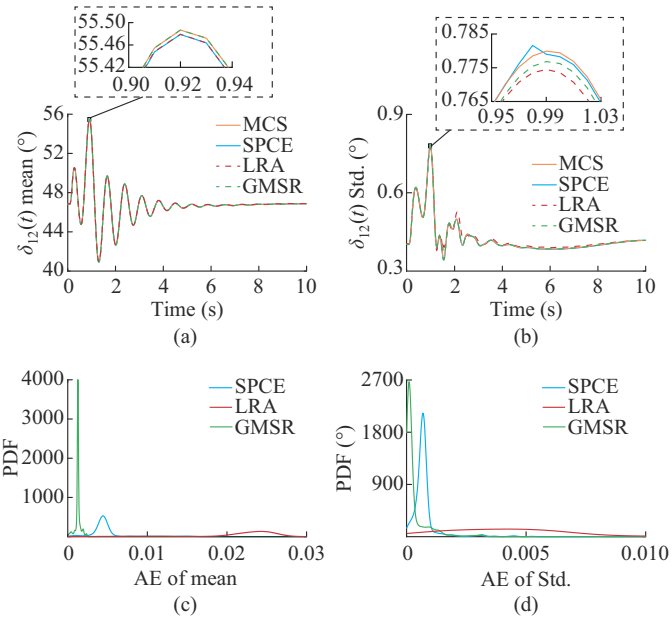

Fig. 6. Accuracy comparison of $\delta_{12}(t)$ moment estimation among various UPA methods. (a) $\delta_{12}(t)$ mean. (b) $\delta_{12}(t)$ Std.. (c) PDF of AE of mean. (d) PDF of AE of Std..

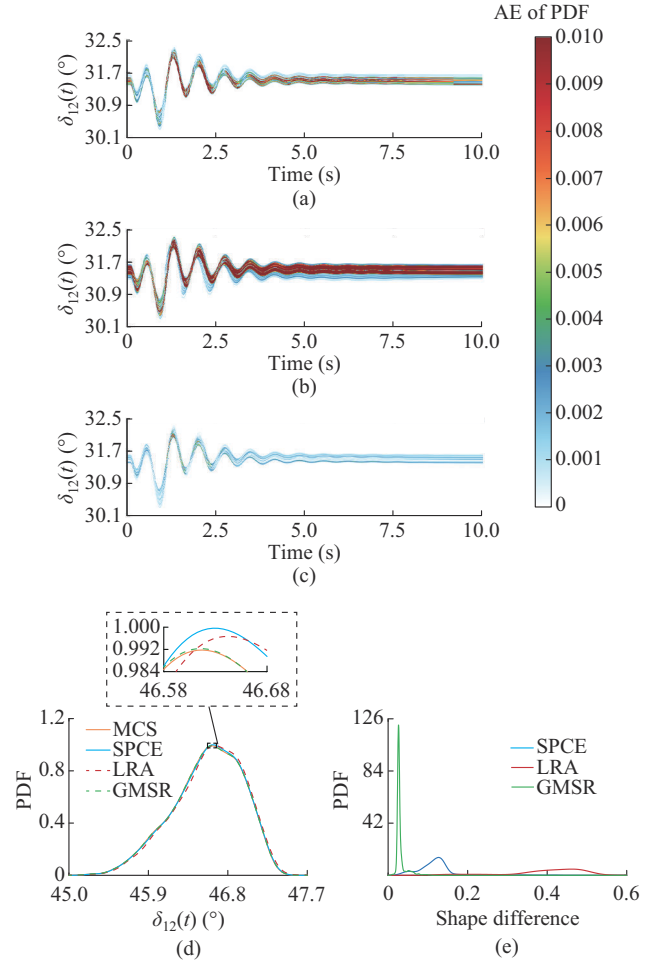

Fig. 7. Accuracy comparison of AE of PDF of $\delta_{12}(t)$ among various UPA methods. (a) AE of PDF of $\delta_{12}(t)$ from SPCE. (b) AE of PDF of $\delta_{12}(t)$ from LRA. (c) AE of PDF of $\delta_{12}(t)$ from GMSR. (d) PDF of $\delta_{12}(t)$ at $t=5$ s. (e) PDF of ε.

Similar to the results in probabilistic frequency stability analysis, from Table II, the total time of GMSR is shorter than those of SPCE and LRA due to the multi-output structure, and the total time of GMSR is significantly shorter than that of MCS since the needed simulation quantity is less. Compared with the total time in probabilistic frequency stability analysis, the method execution time in probabilistic transient stability analysis is very close to that in probabilistic frequency stability analysis, and only the simulation time of them has certain differences. Moreover, though the accuracy of GMSR is not the best at all time points, e.g., the zooming area in Fig. 6(b), the overall accuracy of GMSR is the best. This can be observed based on Figs. 6(c), 6(d), and 7 (e) that the probability distributions of AEs corresponding to the moment and PDF estimation from GMSR are more concentrated to 0 compared with those from SPCE and LRA. Thus, these results demonstrate the superiority of GMSR in efficiency and accuracy of probabilistic transient stability analysis.

B. Case 2: 240-bus WECC System

To verify the scalability and applicability of GMSR in the larger power system with numerous uncertainties, case studies implemented in the 240-bus WECC system are conducted, where 37 renewable energies are integrated [20]. Also, the top 13 loads with the highest active power are selected as uncertainties as cases. Thus, the total uncertainty quantity of renewable energies and loads in the system is 50. These uncertainties are based on the measurements in [21]. Firstly, the proposed uncertainty transformation is carried out. Limited by space, only the correlation coefficients and independence hypothesis among the first 9 uncertainties before and after uncertainty transformation are listed in Table IV. Before uncertainty transformation, the uncertainties have complicated correlations with the maximal correlation coefficient of 0.61 and the minimal correlation coefficient of –0.48. After applying the proposed uncertainty transformation, all uncertainties are independent, which demonstrates the effectiveness of the proposed uncertainty transformation in different uncertainty datasets.

TABLE IV
CORRELATION COEFFICIENTS AND INDEPENDENCE HYPOTHESIS AMONG UNCERTAINTIES BEFORE AND AFTER UNCERTAINTY TRANSFORMATION IN CASE 2

Uncertainty	U1	U2	U3	U4	U5	U6	U7	U8	U9
U1	-	0.09	0.04	0.10	–0.06	0.13	–0.05	0.05	–0.23
U2	0/Y	-	0.44	–0.27	–0.40	–0.19	–0.01	0.08	0.31
U3	0/Y	0/Y	-	–0.32	–0.09	–0.32	0.05	0.05	0.35
U4	0/Y	0/Y	0/Y	-	0.61	–0.16	–0.10	–0.13	–0.33
U5	0/Y	0/Y	0/Y	0/Y	-	–0.31	0.03	0.03	–0.39
U6	0/Y	0/Y	0/Y	0/Y	0/Y	-	–0.48	–0.16	0.05
U7	0/Y	0/Y	0/Y	0/Y	0/Y	0/Y	-	0.39	0.02
U8	0/Y	0/Y	0/Y	0/Y	0/Y	0/Y	0/Y	-	–0.18
U9	0/Y	0/Y	0/Y	0/Y	0/Y	0/Y	0/Y	0/Y	-

Next, probabilistic frequency stability analysis is conducted by using GMSR to analyze the system frequency response $f_{\mathrm{Wsys}}(t)$ and area-level frequency response in Area 1 $f_{\mathrm{Wa1}}(t)$ of the system with the trip of the largest infeed generator at 0.1 s. Firstly, the efficiency comparison of probabilistic frequency stability analysis is presented in Table V. Compared with the total time shown in Table II, the simulation time rises around 4.5 times with the increase of the analyzed system scale. And GMSR, as a nonintrusive method, only needs the data of uncertainties and data of system dynamic responses as inputs and outputs to determine its structure and calculate the coefficients. The method execution time of GMSR rises around 3.5 times with the increase of uncertainty quantity rather than that of analyzed system scale. Moreover, similar total time increase can be found in other methods, and the increase of method execution time of GMSR is limited compared with other methods. Thus, these results demonstrate that GMSR possesses the time-saving merit in UPA of the large-scale power system with numerous uncertainties.

TABLE V
EFFICIENCY COMPARISON OF PROBABILISTIC FREQUENCY STABILITY ANALYSIS IN CASE 2

Method	Simulation time (s)	Method execution time (s)	Total time (s)
MCS	43932.563	-	43932.563
SPCE	1750.381	308.453	2058.834
LRA	1750.381	236.691	1987.072
GMSR	1750.381	8.179	1758.560

Then, the accuracy of methods in estimating the moments and PDFs of frequency responses are compared, as indicated by Figs. 8, 9 and Figs. 10, 11, respectively. From Fig. 8(a) and (c), for mean of frequency responses, all mean curves derived from various methods are very close to the curves from MCS, which illustrates their high accuracy in estimating the mean of frequency responses. Moreover, from Fig. 9(a) and (c), though the peaks of PDFs of AE from LRA are closer to 0 than those from GMSR, the values of their peaks are lower than those from GMSR, and the tails of PDFs of AE from LRA are fatter. This means that the errors of LRA in estimating the mean of frequency responses will fluctuate in a relatively large range compared with GMSR. And for Std. of frequency responses presented in Fig. 9(b) and (d), the peaks of PDFs of AE from GMSR are much higher and closer to 0 compared with those from SPCE and LRA, which means that the Std. curves from GMSR are closer to those from MCS, as shown in Fig. 8(b) and (d). Moreover, for PDFs of frequency responses, it can be clearly observed that AEs of frequency response PDFs from GMSR are much smaller than those from SPCE and LRA, as presented in Fig. 10, and the shape differences of frequency response PDFs from GMSR are also smaller, as illustrated in Fig. 11(b) and (d). These results indicate the high accuracy of GMSR in estimating the moments and PDFs of frequency responses of the large-scale power system with numerous uncertainties.

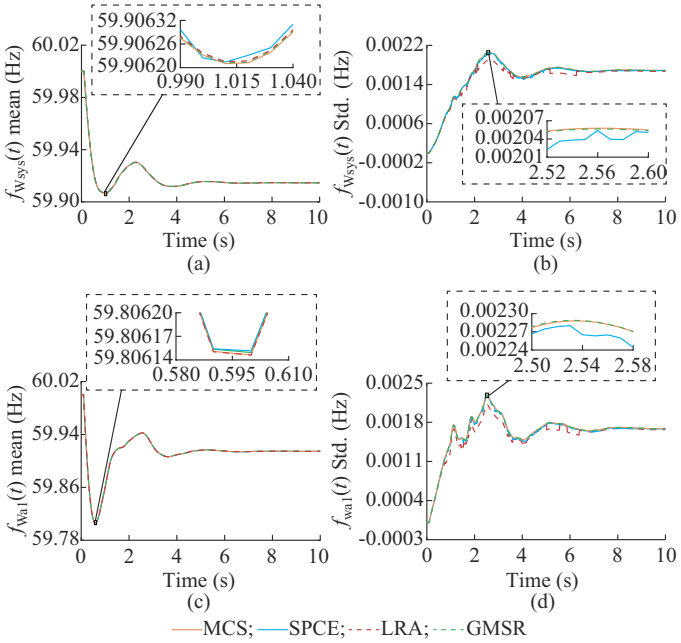

Fig. 8. $f_{\mathrm{Wsys}}(t)$ mean and Std. and $f_{\mathrm{Wa1}}(t)$ mean and Std.. (a) $f_{\mathrm{Wsys}}(t)$ mean. (b) $f_{\mathrm{Wsys}}(t)$ Std.. (c) $f_{\mathrm{Wa1}}(t)$ mean. (d) $f_{\mathrm{Wa1}}(t)$ Std..

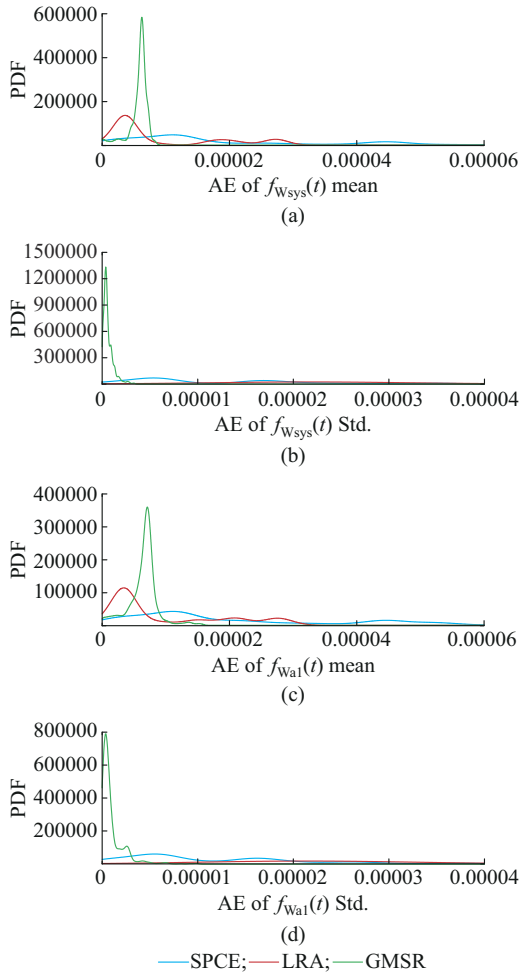

Fig. 9. PDFs of AEs in Case 2. (a) PDF of AE of $f_{\mathrm{Wsys}}(t)$ mean. (b) PDF of AE of $f_{\mathrm{Wsys}}(t)$ Std.. (c) PDF of AE of $f_{\mathrm{Wa1}}(t)$ mean. (d) PDF of AE of $f_{\mathrm{Wa1}}(t)$ Std..

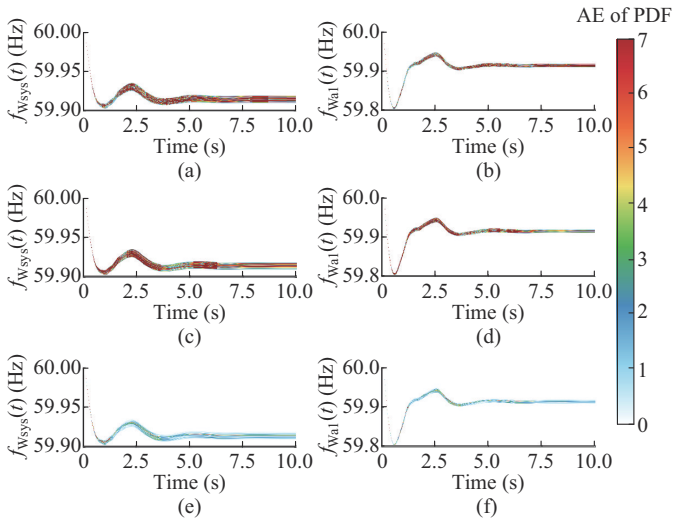

Fig. 10. AEs of PDFs of $f_{\mathrm{Wsys}}(t)$ and $f_{\mathrm{Wa1}}(t)$ in Case 2. (a) AE of PDF of $f_{\mathrm{Wsys}}(t)$ from SPCE. (b) AE of PDF of $f_{\mathrm{Wa1}}(t)$ from SPCE. (c) AE of PDF of $f_{\mathrm{Wsys}}(t)$ from LRA. (d) AE of PDF of $f_{\mathrm{Wa1}}(t)$ from LRA. (e) AE of PDF of $f_{\mathrm{Wsys}}(t)$ from GMPR. (f) AE of PDF of $f_{\mathrm{Wa1}}(t)$ from GMPR.

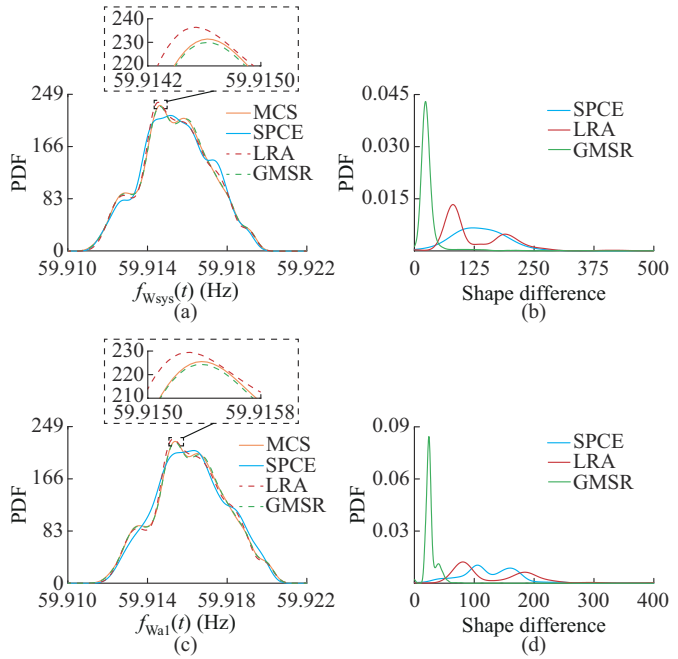

Fig. 11. PDFs of $f_{\mathrm{Wsys}}(t)$, $f_{\mathrm{Wa1}}(t)$, and ε of $f_{\mathrm{Wa1}}(t)$ in Case 2. (a) PDF of $f_{\mathrm{Wsys}}(t)$ at $t=5$ s. (b) PDF of ε of $f_{\mathrm{Wsys}}(t)$. (c) PDF of $f_{\mathrm{Wa1}}(t)$ at $t=5$ s. (d) PDF of ε of $f_{\mathrm{Wa1}}(t)$.

IV. Conclusion

This paper proposes a GMSR method for UPA of power system dynamics. The simulation results demonstrate that the data-driven uncertainty transformation can effectively transform realistic uncertainties with complicated correlations and probability distributions into uncorrelated and independent ones, which can be integrated into other SR-based UPA methods as a widely used preprocessing. Moreover, compared with existing nonintrusive SR-based UPA methods, GMSR significantly improves the efficiency and accura-

cy in analyzing probabilistic frequency and transient stability. Since the proposed GMSR is nonintrusive, it can be easily applied to other probabilistic stability issues related to power system dynamics. Additionally, in this paper, some GMSR parameters are selected based on existing studies. However, they may affect the performance of GMSR in different scenarios. Also, since the inputs and outputs of GMSR are data, when they are influenced by noises, GMSR accuracy will be affected. Thus, further studies will focus on parameter selection optimization and data preprocessing in filtering distorted data or restoring original data to improve the applicability and robustness of GMSR. Additionally, as a generic method, GMSR has the potential to be extended to UPA of multiple stability indices simultaneously and the design of probabilistic stability enhancement strategies.

REFERENCES

[1] K. N. Hasan, R. Preece, and J. V. Milanović, "Existing approaches and trends in uncertainty modelling and probabilistic stability analysis of power systems with renewable generation," *Renewable and Sustainable Energy Reviews*, vol. 101, pp. 168-180, Mar. 2019.

[2] A. M. Hakami, K. N. Hasan, M. Alzubaidi *et al*., "A review of uncertainty modelling techniques for probabilistic stability analysis of renewable-rich power systems," *Energies*, vol. 16, no. 1, p. 112, Dec. 2023.

[3] M. Aien, M. Fotuhi-Firuzabad, and F. Aminifar, "Probabilistic load flow in correlated uncertain environment using unscented transformation," *IEEE Transactions on Power Systems*, vol. 27, no. 4, pp. 2233-2241, Nov. 2012.

[4] M. Aien, A. Hajebrahimi, and M. Fotuhi-Firuzabad, "A comprehensive review on uncertainty modeling techniques in power system studies," *Renewable and Sustainable Energy Reviews*, vol. 57, pp. 1077-1089, May 2016.

[5] Z. Wang and S. Bu, "Probabilistic frequency stability analysis considering dynamics of wind power generation with different control strategies," *IEEE Transactions on Power Systems*, vol. 39, no. 5, pp. 6412-6425, Sept. 2024.

[6] M. Fan, Z. Li, T. Ding *et al.*, "Uncertainty evaluation algorithm in power system dynamic analysis with correlated renewable energy sources," *IEEE Transactions on Power Systems*, vol. 36, no. 6, pp. 5602-5611, Apr. 2021.

[7] K. Ye, J. Zhao, N. Duan *et al*., "Stochastic power system dynamic simulation and stability assessment considering dynamics from correlated loads and PVs," *IEEE Transactions on Industry Applications*, vol. 58, no. 6, pp. 7764-7775, Nov. 2022.

[8] Y. Xu, L. Mili, A. Sandu *et al*., "Propagating uncertainty in power system dynamic simulations using polynomial chaos," *IEEE Transactions on Power Systems*, vol. 34, no. 1, pp. 338-348, Jan. 2019.

[9] B. Xia, H. Wu, Y. Qiu *et al*., "A Galerkin method-based polynomial approximation for parametric problems in power system transient analysis," *IEEE Transactions on Power Systems*, vol. 34, no. 2, pp. 1620-1629, Mar. 2019.

[10] L. Li, Y. Qiu, H. Wu *et al*., "Uncertainty analysis of power system time-domain simulation based on generalized polynomial chaos method," in *Proceedings of 2017 IEEE PES General Meeting (PESGM)*, Chicago, USA, Jul. 2017, pp. 1-5.

[11] X. Wang, R. Liu, X. Wang *et al*., "A data-driven uncertainty quantification method for stochastic economic dispatch," *IEEE Transactions on Power Systems*, vol. 37, no. 1, pp. 812-815, Jan. 2022.

[12] X. Wang, X. Wang, H. Sheng *et al*., "A data-driven sparse polynomial chaos expansion method to assess probabilistic total transfer capability for power systems with renewables," *IEEE Transactions on Power Systems*, vol. 36, no. 3, pp. 2573-2583, May 2021.

[13] Neon Neue Energieökonomik, Technical University of Berlin, ETH Zürich, and DIW Berlin. (2024, Nov.). OPSD data packages. [Online]. Available: https://open-power-system-data.org/

[14] B. Chen, S. Yim, H. Kim *et al*., "Cybersecurity of wide area monitoring, protection, and control systems for HVDC applications," *IEEE Transactions on Power Systems*, vol. 36, no. 1, pp. 592-602, Jan. 2021.

[15] A. Hyvärinen and E. Oja, "Independent component analysis: algorithms and applications," *Neural Networks*, vol. 13, no. 4, pp. 411-430, Jun. 2000.

[16] X. Xing, J. Ge, W. Peng *et al.*, "Independent component analysis (ICA) based method for estimating the deformation of highways in permafrost region (HPICA) – a case study of maduo section of gongyu highway," *IEEE Journal of Selected Topics in Applied Earth Observations and Remote Sensing*, vol. 17, pp. 970-984, Dec. 2023.

[17] A. Akrami and H. Mohsenian-Rad, "Event-triggered distribution system state estimation: sparse Kalman filtering with reinforced coupling," *IEEE Transactions on Smart Grid*, vol. 15, no. 1, pp. 627-640, Jan. 2024.

[18] J. Wen, S. Bu, and F. Li, "Two-level ensemble methods for efficient assessment and region visualization of maximal frequency deviation risk," *IEEE Transactions on Power Systems*, vol. 38, no. 1, pp. 643-655, Jan. 2023.

[19] Z. Wang and S. Bu, "Design and defense of modal resonance-oriented cyber-attack against wide-area damping control," *IEEE Transactions on Smart Grid*, vol. 15, no. 2, pp. 2164-2178, Mar. 2024.

[20] H. Yuan, R. S. Biswas, J. Tan *et al*., "Developing a reduced 240-bus WECC dynamic model for frequency response study of high renewable integration," in *Proceedings of 2020 IEEE/PES Transmission and Distribution Conference and Exposition (T&D)*, Chicago, USA, Oct. 2020, pp. 1-5.

[21] California ISO. (2024, Nov.). Managing the evolving grid. [Online]. Available: https://www. caiso. com/about/our-business/managing-the-evolving-grid

Zhaoyuan Wang received the B.S. degree in electrical engineering and its automation from North China Electric Power University, Baoding, China, in 2018, and the M.S. degree in electrical engineering from Huazhong University of Science and Technology, Wuhan, China, in 2021. He is currently pursuing the Ph.D. degree with the Department of Electrical and Electronic Engineering, The Hong Kong Polytechnic University, Hong Kong, China. His current research interests include uncertainty quantification of renewable penetrated power system and stability analysis of cyber-physical power system.

Siqi Bu received the Ph.D. degree from the electric power and energy research cluster, The Queen's University of Belfast, Belfast, UK, where he continued his postdoctoral research work before entering industry. Then, he was with National Grid UK as an experienced UK National Transmission System Planner and Operator. He is an Associate Professor and Associate Head with Department of Electrical and Electronic Engineering, The Hong Kong Polytechnic University, Hong Kong, China, and also a Chartered Engineer with UK Royal Engineering Council, London, UK. His research interests include power system stability, operation, and economics considering renewable energy integration, smart grid application, and transport electrification.